nature photonics

SUPPLEMENTARY INFORMATION

DOI: 10.1038/NPHOTON.2015.105

Macroscopic and Direct Light Propulsion of Bulk Graphene Material

Tengfei Zhang[1†], Huicong Chang[1†], Yingpeng Wu[1†], Peishuang Xiao[1], Ningbo Yi[1], Yanhong Lu[1], Yanfeng Ma[1], Yi Huang[1], Kai Zhao[1], Xiao-Qing Yan[2], Zhi-Bo Liu[2], Jian-Guo Tian[2], Yongsheng Chen[1*]

[1]Key Laboratory of Functional Polymer Materials and Center for Nanoscale Science and Technology, Collaborative Innovation Center of Chemical Science and Engineering, Institute of Polymer Chemistry, College of Chemistry, Nankai University, Tianjin 300071, China.

[2]Key Laboratory of Weak Light Nonlinear Photonics, Ministry of Education, Teda Applied Physics School and School of Physics, Nankai University, Tianjin 300457, China.

*Correspondence to: yschen99@nankai.edu.cn

This PDF file includes:

DOI: 10.1038/NPHOTON.2015.105

Materials Synthesis

Commercial materials are used directly for general chemicals unless otherwise indicated. Graphene Oxide (GO) was prepared by the oxidation of natural graphite powder using a modified Hummer's method, as described elsewhere[1]. A low concentration GO ethanol solution (0.375 mg ml^{-1}) was solvothermally treated in a Teflon-lined autoclave at 180 °C for 12 h, then the ethanol-filled intermediate solid was carefully removed from the autoclave to have a slow solvent exchange with water. After the solvent exchange process was totally completed, the water-filled sponge was freeze-dried. Finally, the sponge was annealed at 800 °C for an hour in argon atmosphere to obtain the final graphene sponge.

Instruments and Measurements Conditions

The laser devices used in our experiment were purchased from Shaanxi Alaxy Technologies Photonics Company, these includes models of PT-LD-650-1W, PT-DPL-532-1W, PT-LD-650-3W-FCL, PT-DPL-532-3W-FCL, and PT-DPL-450-3W-FCL. The laser power meter was Ophir Nova II and the laser power sensor was Ophir thermal power/energy laser measurement sensor 10A-P. The short-arc xenon lamp was CHF-XM500 obtained from the Beijing Changtuo Technology Company. A Solarimeter SM206 from the Shenzhen Xinbaorui Instruments Company was used to measure the radiation intensity of simulated sunlight and real sunlight. In some cases, Baader Planetariums AstroSolar TM safety film was used to reduce the radiation intensity for measuring the light intensity. The precision current measurement was carried out using a Keithley 2400 Digital Source Meter, and Rigol DS1102E digital oscilloscope (1 GSa s^{-1},

100 MHz) was also used for the current signal measurement. The molecular pump unit was PFJ-100 from Beijing Pator Vacuum Technology Company. The tachometer to measure the rotation speed was a CEM AT-6 from Shenzhen Huashengchang Company. The electronic balance used was a Sartorius BT25S.

Elemental Analysis (EA) was performed at an ELEMENTAR Vario Micro elemental analyzer for determination of the C, H and O content. Scanning Electron Microscopy (SEM) images were obtained on a JEOL JSM-7500F scanning electron microscope using an accelerating voltage of 5 KV or 20 kV, and Energy Dispersive X-Ray Spectroscopy (EDS) was obtained by the OXFORD EDS detect module. Transmission Electron Microscopy (TEM) was conducted in a FEI Tecnai G2 F20 electron microscope using an acceleration voltage of 200 kV. Samples for TEM analysis were prepared by sonicating graphene sponge in ethanol and then dropping the supernate onto a Cu micro grid and drying in air. X-ray Photoelectron Spectroscopy (XPS) to analyze the chemical composition of the graphene sponge was carried out using an AXIS HIS 165 spectrometer (Kratos Analytical) with a monochromatized Al Kα X-ray source (1486.6 eV). Auger electron spectroscopy (AES) was obtained with a ULVAC-PHI PHI-700Xi Scanning Auger Nanoprobe. The spectrometer was equipped with a coaxial electron gun and Cylindrical Mirror Analyzer (CMA). X-Ray Diffraction (XRD) measurements were carried out on a Rigaku D/Max-2500 diffractometer using Cu Kα radiation. Raman spectra were examined with a Renishaw InVia Raman spectrometer using laser excitation at 514.5 nm. Lorentzian fitting was carried out to obtain the positions, widths and areas of the D, G, 2D and (D + G) peaks of graphene in its Raman spectra. Fourier Transform Infrared Spectroscopy (FT-IR) spectra were obtained using a

DOI: 10.1038/NPHOTON.2015.105

BRUKER Tensor 27 FT-IR Spectrometer. Visible Diffuse Reflection Spectra (Vis-DRS) were obtained using JASCO V-570 Spectrophotometer and the diffuse reflection mode was chosen.

All the mass spectra were obtained using a 7.0 T Fourier Transform Ion Cyclotron Resonance Mass Spectrometer (FTICR MS) instrument (mass/charge resolution better than 0.07) with a Matrix-Assisted Laser Desorption Ionization (MALDI) source (VarianIonSpec ProMALDI) and a non-commercial Atmospheric Negative-Ion Orthogonal Acceleration Time-of-Flight (OA-TOF) Mass Spectrometer (mass/charge resolution better than 0.05). In our test of using MALDI-FTICR mass spectrometer, the pulse laser of MALDI source was closed off and our laser was used to illuminate the sample which was placed in the vacuum sample chamber of the mass spectrometer, both the positive and negative measurement modes were tested, and the complete mass/charge detection range was 150-4000 (corresponding mass range of 150-4000 amu). Lasers with different wavelengths (450, 532 and 650 nm) were used to illuminate the sample. The result of followed conditions was shown in Supplementary Fig. 11: laser wavelength, 450 nm; laser power, 1.7 W; laser spot area, 4 mm^2; test mode, positive; mass/charge detection range, 216-4000. Tests with different combinations of conditions gave the similar results and conclusions, and they were not shown here. In our test of using the non-commercial OA-TOF mass spectrometer, the graphene sponge was placed in a special sample chamber with N_2 atmosphere and it could be illuminated by laser through a window on the chamber. The chemical ionization source was removed and repulsion electrode was retained. The instrument could detect negative ion and the mass/charge

detect range was about from 12 to 321. The 450 nm laser (2 W; laser spot area, 4 mm^2) was used to illuminate the samples and the result was shown in Supplementary Fig. 12.

The emitted electron kinetic energy spectra were obtained using a PHI Quantera XPS spectrometer instrument. The graphene sponge sample was fixed on a moveable sample platform. The laser replacing the original X-ray source inside the instrument was used to illuminate the sample through the observation window. A kinetic energy distribution spectrum of electrons emitted from the graphene sponge under the laser illumination was collected by a Concentric Hemispherical Electron Energy Analyzer (CHA) equipped with the XPS instrument. The acquisition time of the spectra was 2.0 min, and blank noise signal collection was done under the same conditions only without laser illumination. The vacuum of the XPS instrument was better than 6.7×10^{-9} Torr.

Supplementary Discussion

Rotation Speed and Rotational Kinetic Energy

All the rotation speed data was record by a non-contact tachometer under given laser wavelength, laser power density and graphene sample. When illuminated with laser, the rotation speed increased initially and a max speed was achieved after a few seconds due to the friction force. The max speed was then recorded and used. Such testing was repeated for 10-15 times and all the max rotation speed data was averaged and then used for the following calculation. With the following equations: $E_r = \frac{1}{2} I\omega^2$, $\omega = 2\pi n/60$, the rotational kinetic energy of the sample E_r was proportional to square of angular velocity ω, and the angular velocity ω was proportional to rotation speed n in rpm, I was the rotational inertia, so the rotational kinetic energy E_r was proportional to square of

DOI: 10.1038/NPHOTON.2015.105

rotation speed too. From the point of energy conversion, the square of the rotation speed (thus the rotational kinetic energy of the sample) should have a linear quantitative relationship with the laser power density/wavelength under the same testing conditions. Note when the work of the driving force did was equal to the work of frictional force did in every round, the rotation speed would not increase anymore and the maximum rotation speed could be reached. The frictional force is proportional to the pressure force generated by the sample on the axis during the rotation, and such pressure force was proportional to square of angular velocity. The driving force should be constant with a given laser wavelength and laser power density (with the same laser spot area) for the same sample. Based on all above discussions, the square of rotation speed should have a linear relationship with the laser power density/wavelength for the same sample.

Calculation of Radiation Pressure

The radiation pressure can be calculated through the classical Maxwell electromagnetism (wave model) or quantum mechanics (photon model), and both theories give the same equation: $P = I(2R + A)/\mathrm{c}$, where P is the pressure, I is energy flux (intensity) in W m^{-2}, R is the surface reflectivity of the body, A is the surface absorptivity of the body, and c is speed of light in vacuum[2,3]. As in our case, the transmissivity (T) of the graphene sponge is zero, so the reflectivity R and absorptivity A satisfy the equation $R + A = 1$, then the aforementioned radiation pressure equation could be simplified as $P = I(\mathrm{R}+1)/\mathrm{c}$. The radiation pressure under 0 AM (Air Mass) standard solar light (1361 W m^{-2} at 1 Astronomical Unit (AU)[4]) is 9.08 μN m^{-2} or less which depends on the reflectivity, making it an extremely low thrust propulsion system[5]. In our laser-induced motion, a typical and simplified estimation is as follows: the laser power is

about 1 W and the light spot area is about 4 mm^2 (light intensity is 1 W/4 mm^2 = 2.5 × 10^5 W m^{-2}), the *R* value is determined to be 0.05, as the graphene sponge has a quite low reflectivity in the visible wavelengths from 400 to 800 nm by Visible Diffuse Reflection Spectra (Vis-DRS) shown in Supplementary Fig. 17. Then the light pressure should be 2.5 × 10^5 W m^{-2} × (0.05 +1) / 3 × 10^8 m s^{-1} = 875 μN m^{-2}, corresponding to a propulsion force of 3.50 × 10^{-9} N considering of laser spot area. Such a small force is several orders of magnitude smaller than the gravity of a typical graphene sponge sample (9.8 × 10^{-7}–9.8 × 10^{-6} N for the mass at 0.1–1 mg). Similarly, for the simulated sunlight situation, a typically light intensity could be ~1100 mW cm^{-2} (1.1 × 10^4 W m^{-2}) and the illumination area is ~7.85 × 10^{-5} m^2, so the radiation pressure of simulated sunlight should be 38.5 μN m^{-2} and the propulsion force should be ~3.02 × 10^{-9} N. It is also several orders of magnitude smaller than the gravity of a typical graphene sponge sample (9.8 × 10^{-7}–9.8 × 10^{-6} N for the mass at 0.1–1 mg).

No Weight Reduction of Graphene Sponge under Laser Illumination

A graphene sponge sample was weighed carefully for several times and the results were averaged. Then the sample was put in a vacuum tube and illuminated by a laser (450 nm, 2 W and laser spot area of 4 mm^2) for propulsion. Such operation was repeated for at least 40 times. Then the sample was taken out of the vacuum tube and weighed again carefully. There was no weight reduction of graphene sponge after so many times of laser-induced propelled operation. The accuracy of the electronic balance is ± 0.01 mg. The graphene sample weight is at least 3 mg. Several samples were tested under the same process and gave the same result.

Mathematical Calculation of the Average Current Signal Intensity

DOI: 10.1038/NPHOTON.2015.105

By using the device showed in Fig. 4a, we could obtain a real-time Current-Time curve under a given laser wavelength and laser power density (one such curve was showed in Fig. 4b). Then we could obtain the integral of current versus time by software (the integral of background current noise versus time was deducted). Because the frequency and geometry of mechanical chopper was known, so the actual illumination time could be calculated. The average current intensity could then be obtained by dividing the integral result by actual total illumination time. Such average current intensity results were obtained from repeating tests and the results were averaged again and used for the plotting under a given laser power density and laser wavelength. Standard deviation was calculated from these data too and was shown in the corresponding figures such as in Fig. 4c and Supplementary Fig. 14. Based on the average current intensity, corresponding electron emission rate could be calculated through dividing by the charge of single electron (1.60×10^{-19} C).

The Possible Highest Temperature of the Graphene Sponge Sample under Illumination of Laser Pulse

The absorbance of a single layer graphene is 2.3 % (Reference S6), so after passing through 400 layers graphene, the intensity of the light is ~0.01 % of the initial light intensity and we can assume that the light is absorbed totally (assuming the reflection is negligible). With the 2D mass density (7.6×10^{-8} g cm^{-2}) of graphene[7,8], the total graphene mass illuminated (reached) by laser under the laser spot is simply estimated as (7.6×10^{-8} g cm^{-2}) × (400 layers) × (4 mm^2) × 3 = 3.65×10^{-3} mg, the factor 3 is used to factor in all the graphene sheets in the x, y, z directions and 4 mm^2 is the laser spot area. The specific heat capacity of graphene is ~ 2 J g^{-1} k^{-1} (Reference S9–S11). With the laser

pulse width of 2 ms and the laser power at 3 W, the energy of a single laser pulse is 6 mJ. If all the photo energy of one laser pulse transforms into heat completely and without any heat loss to the surrounding environment (and the graphene), the part of graphene sponge in this region of laser spot can obtain a temperature increasement of about 6 mJ/(3.65 × 10^{-3} mg × 2 J g^{-1} K^{-1}) = 822 K. This indicates the highest temperature of the sample is lower than 900 °C. This temperature is significantly lower than the temperature required for thermionic electron emission of graphene.

Estimation of the Energy Conversion in the Laser-induced Propulsion and Rotation

For the laser-induced vertical upwardly propulsion and sake of easy estimation, the propulsion force is assumed to be constant with a given laser wavelength and laser power density at the initial stage (taking off). So an ideal laser-induced propulsion should be uniformly accelerated motion in this stage where the friction force is not applied yet. And as discussed in the main text, the entire propulsion process was affected by other factors such as electrostatic attraction and irregular friction, so we only picked a short time (the initial taking off stage) after the laser illuminated on the graphene sample to analyze the problem.

In the uniformly accelerated motion:

$$s = V_0 t + \tfrac{1}{2} a t^2,\ v_t = V_0 + at$$

Where the s is the distance, V_0 is the initial speed, t is the time, a is the acceleration, and v_t was the speed when time equal to t. In our case, $V_0 = 0$ and $s = h$, where the h is height. So:

$$v_t = 2h / t$$

For the whole (the initial taking off) process:

DOI: 10.1038/NPHOTON.2015.105

$$W_p = mgh + \tfrac{1}{2}mv_t^2$$

Where W_p was the work done by propulsion force in the whole initial taking off stage process, m was the sample mass, g was the gravitational acceleration.

We obtained three groups of data from videos of laser-induced vertical upwardly propulsion and listed them as follows:

m (mg)	t (s)	h (cm)
0.60	1/50	1.0
0.08	2/30	2.1
0.85	2/30	2.7

So the W_p was 3.6×10^{-7}, 3.2×10^{-8}, 5.0×10^{-7} J, respectively, and the corresponding power was 3.6×10^{-5}, 4.8×10^{-7}, 7.5×10^{-6} W, respectively. Such a big difference may be caused by the factors such as electrostatic attraction and irregular friction in the propulsion process and the over simplified model.

The rotation of graphene sponge could be estimated with the variable accelerated rotation model. Based on the equations as follows:

$$E_r = \tfrac{1}{2}I\omega^2,\ I = \tfrac{1}{12}m\left(l_1^2 + l_2^2\right),\ \omega = 2\pi n/60$$

Where E_r was the rotational kinetic energy, I was the rotational inertia of the sample, ω was the angular velocity, m was the sample mass, l_1 and l_2 were edge lengths of the edges which were perpendicular to the axis of rotation, n was the rotation speed in rpm. For a typical graphene sponge, m = 0.44 mg, l_1 = 12 mm, l_2 = 7 mm, based on the measured rotation speed at about 2700–15000 rpm, the rotational kinetic energy could be obtained at about 2.9×10^{-7}–9.2×10^{-6} J.

In the main text, we have calculated that the power produced by the ejected electrons was about 6.4×10^{-5}–2.2×10^{-6} J s^{-1} (Watt). Such a power/energy was large enough to support the laser-induced propulsion/rotation by comparing with the above discussion.

DOI: 10.1038/NPHOTON.2015.105

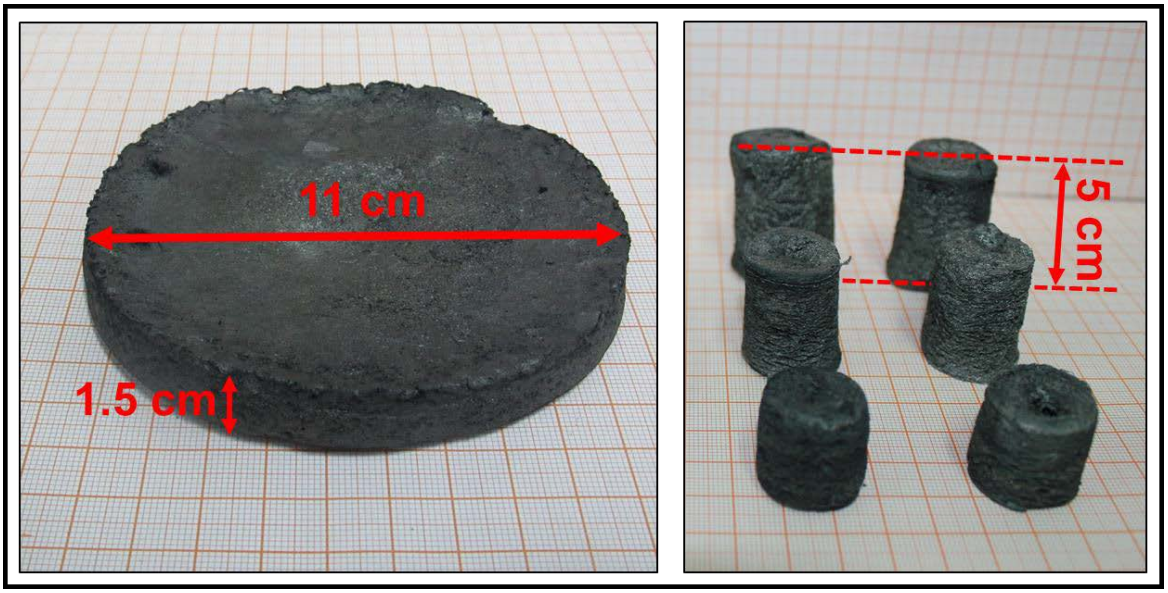

Figure S1

The photographs of as-prepared graphene sponges with different sizes and shapes, and the volume of the graphene sponge in the left was larger than 140 cm^3.

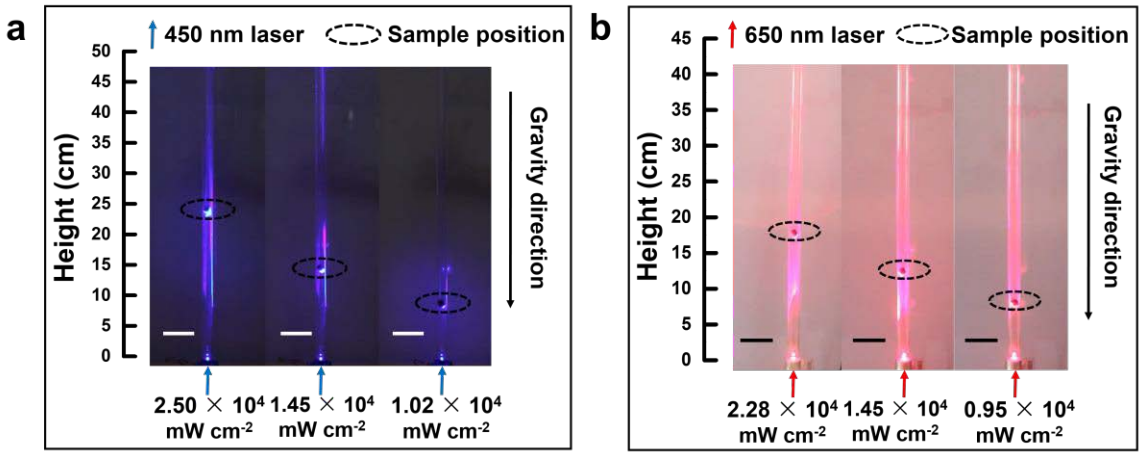

Figure S2

a, The propulsion height of the same sample illuminated by the 450 nm laser at different power density (Scale bars, 5 cm). **b,** The propulsion height of the same sample illuminated by the 650 nm laser at different power density (Scale bars, 5 cm). The pictures were all screenshots at the same moment of 1 s from the videos. They show that the propulsion height increases with the increasing laser power density if the laser wavelength is fixed. The sample in **(a)** and **(b)** was placed in a vertical vacuum tube, and the vacuum was 6.8×10^{-4} Torr. The diameter and height of the cylinder shape sample were 10 and 11 mm respectively, and the mass of the sample was 0.86 mg. The laser spot areas were all ~4 mm^2.

DOI: 10.1038/NPHOTON.2015.105

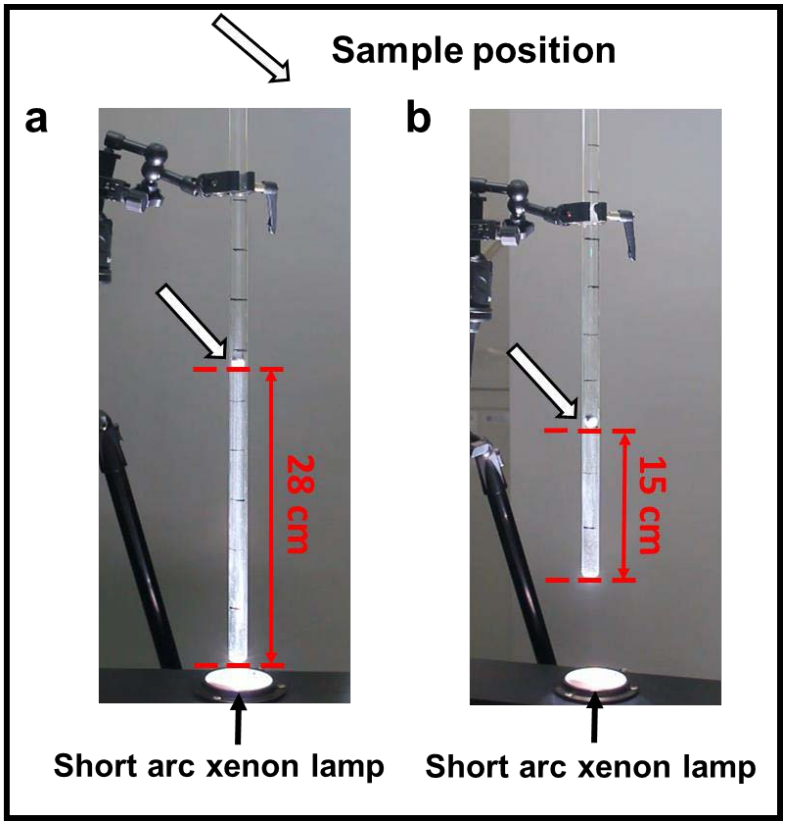

Figure S3

The different propulsion heights when varying the initial distance between Xenon lamp (light source) and graphene sponge sample. The distances were 8.5 cm in **(a)** and 18.5 cm in **(b)**, and the light intensity at the initial position was ~ 4200 mW cm^{-2} and ~ 1100 mW cm^{-2} respectively. This demonstrates that stronger light intensity (smaller distance between light source and graphene sponge sample) leads to more effective light propulsion which is similar when laser light source was used. The pictures were all screenshots at the moment of 1 s from the videos. The sample in **(a)** and **(b)** was placed in a vacuum tube, and the vacuum was 6.8×10^{-4} Torr. The diameter and height of the cylinder shape sample were 10 and 11 mm respectively, and the mass of the sample was 0.87 mg.

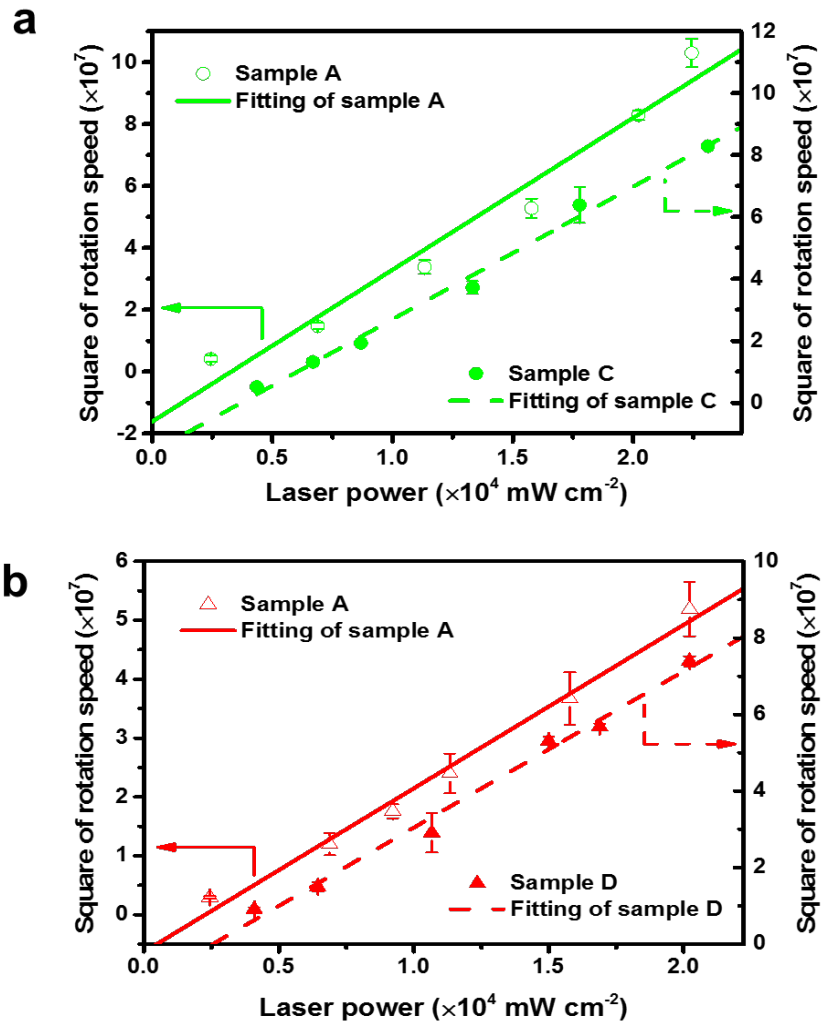

Figure S4

The dependence of laser power density on the square of rotation speed for different samples: **(a)** sample A and C, 532 nm laser; **(b)** sample A and D, 650 nm laser. With the same sample and laser wavelength, the square of rotation speed increases linearly with the laser power density. The error bars in **(a)** and **(b)** were the variance S^2 of rotation speed data. Sample A: 12.5 × 8 × 3.5 mm^3, 0.36 mg. Sample C: 11 × 6.4 × 4 mm^3, 0.29 mg. Sample D: 11 × 6 × 4 mm^3, 0.27 mg. All the experiments were carried out in the vacuum of 6.8×10^{-4} Torr. The laser spot areas were all about 4.5 mm^2.

DOI: 10.1038/NPHOTON.2015.105

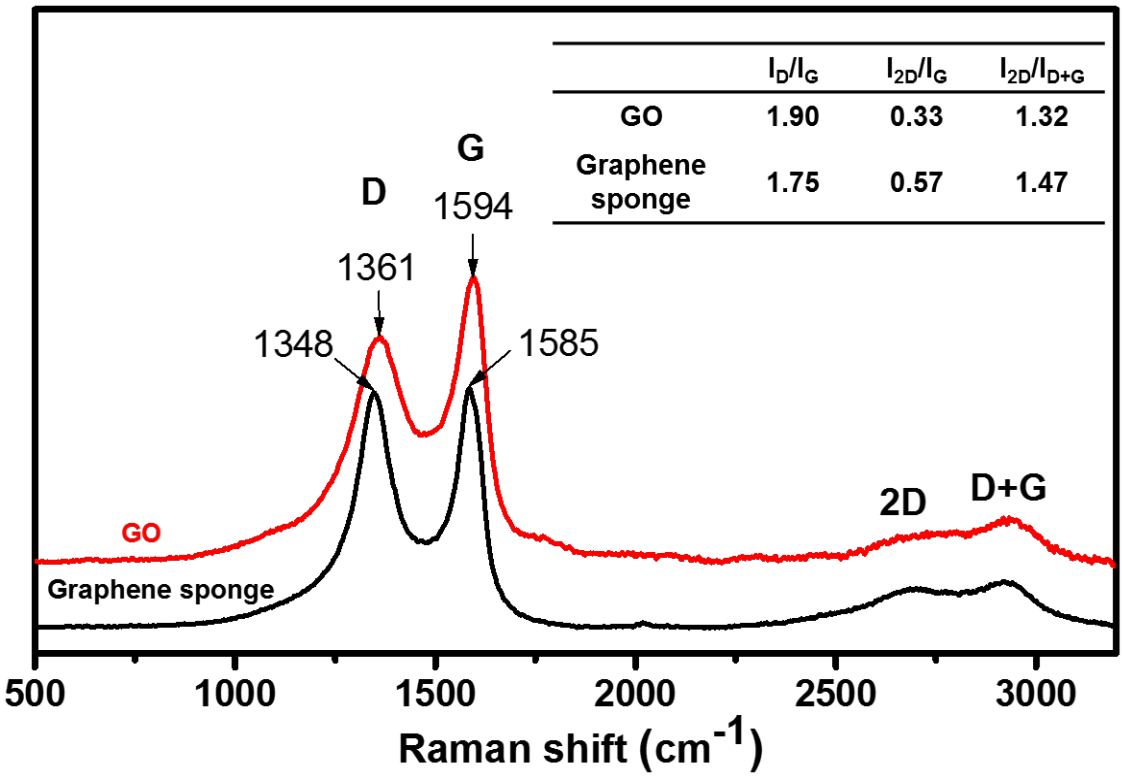

Figure S5

The Raman spectra of the GO (red line) and the graphene sponge (black line). Lorentzian fitting was carried out to obtain the positions, widths and areas of the D, G, 2D and (D + G) peaks in the Raman spectra. When compared with GO, the integrated peak area ratio of the D and G peaks I_D/I_G decreased, which indicates the increasement of sp^2 domain size. The increasement of I_{2D}/I_G and I_{2D}/I_{D+G}, combining with downshift to a lower energy of graphene sponge's G band, also suggests graphitic "self-healing" or the recovery of π electronic conjugation for graphene sponge in the 800 °C annealing process[12–17].

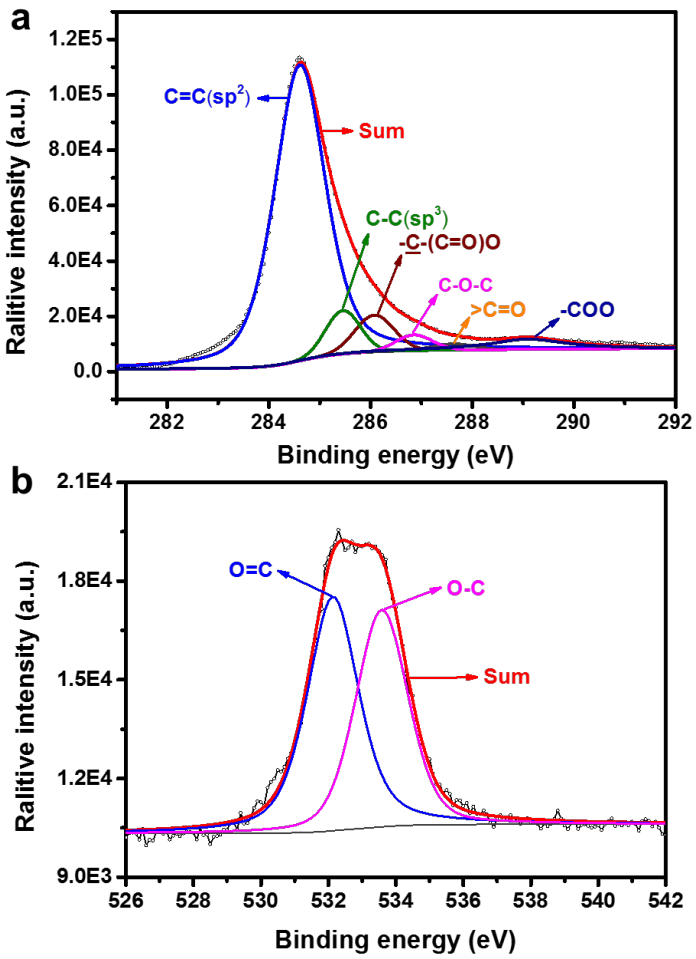

Figure S6

The XPS spectra of the C 1s and O 1s peaks of the graphene sponge. **(a)** C 1s peak spectrum indicates that the graphene sponge is dominant with sp^2 carbon (~ 284.6 eV), and also a small amount of other carbon atoms existing in the forms of ether C-O (~ 286.8 eV) and ester C(=O)O (~ 288.9 eV) bonds. The assignment of the peaks around 285-286 eV could be arguable because of the very complicated structure of the material. **(b)** The O 1s peak showed that the oxygen element had two forms: O=C and O-C at 532.1 and 533.6 eV respectively[18–21], though the exact assignment could also be complicated similarly as in the C 1s case above.

DOI: 10.1038/NPHOTON.2015.105

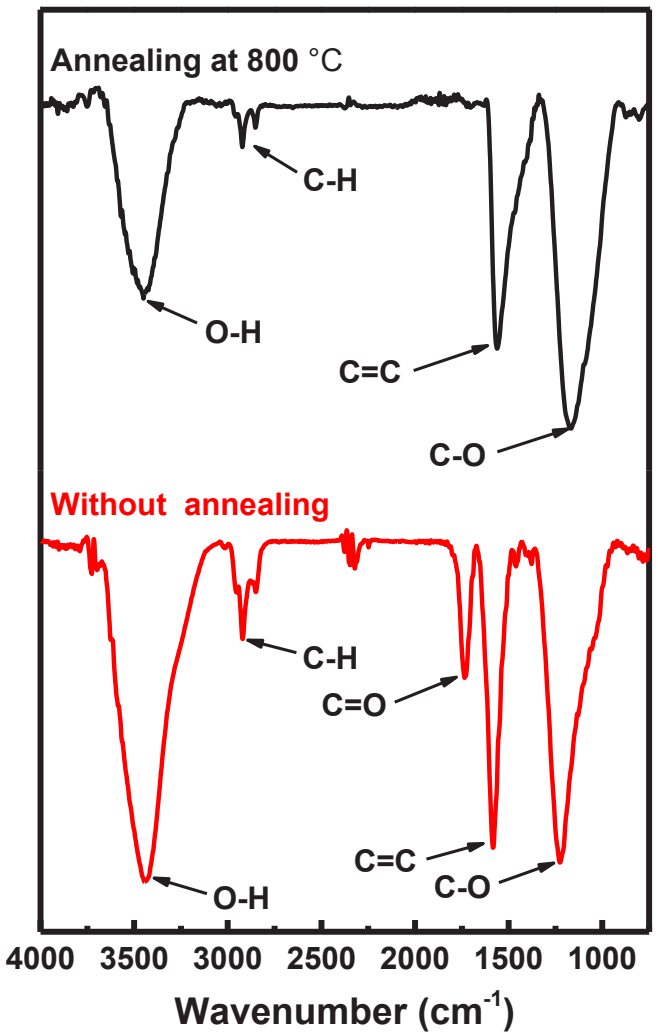

Figure S7

The IR spectra of the graphene sponge annealing at 800 °C (black line) and without annealing (red line). The appearance of C-O peak indicates that there was C–O–C covalent bonds in the graphene sponge even after annealing[22]. The C=O peak of graphene sponge after annealing decreased significantly and nearly disappeared, and such phenomenon should be caused by the removal of most C=O bond in the annealing process. The O–H peak at 3430 cm^{-1} is mainly assigned to external absorbed water from air.

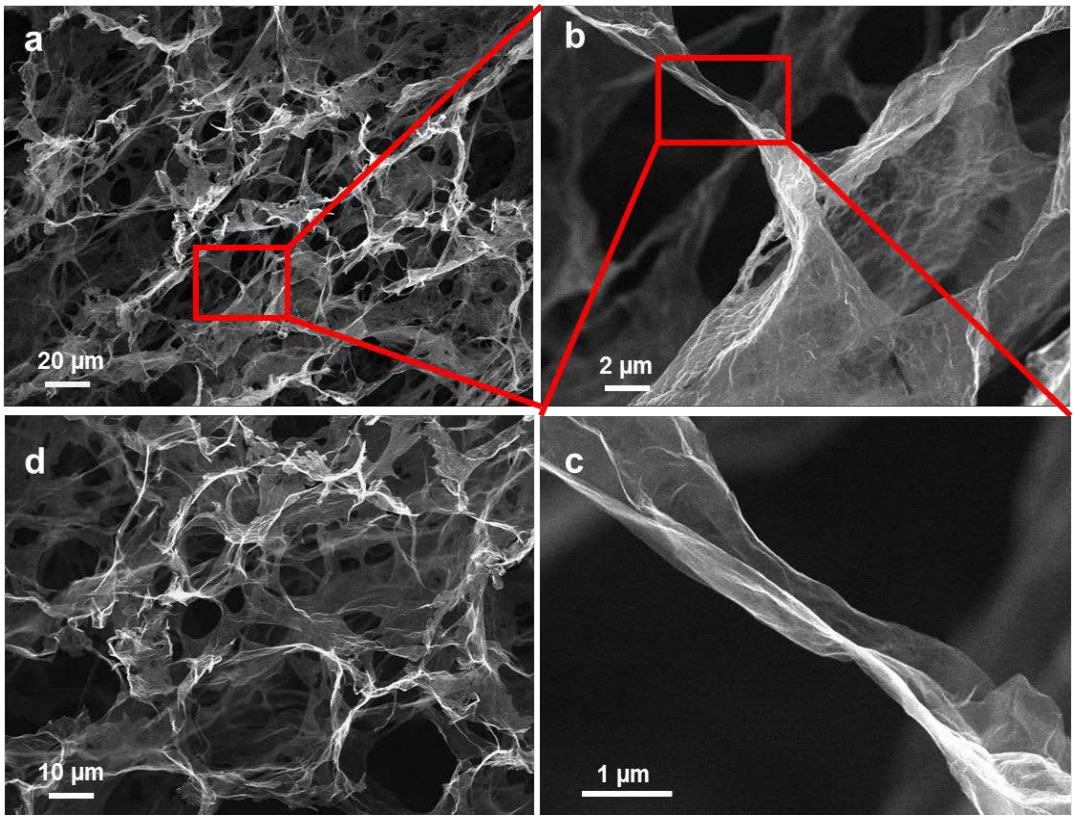

Figure S8

The SEM images of the graphene sponge **(a)** and **(d)** shows it is highly porous material of graphene. **(b)** is the enlarged image of labeled zone in **(a)** and shows that the cross-linked part of the graphene walls. **(c)** is the enlarged image of labeled zone in **(b)**, which shows that the pore wall is made of the graphene sheets. **(d)** was also the analysis region for EDS and the corresponding EDS results are summarized in Supplementary Table 1.

DOI: 10.1038/NPHOTON.2015.105

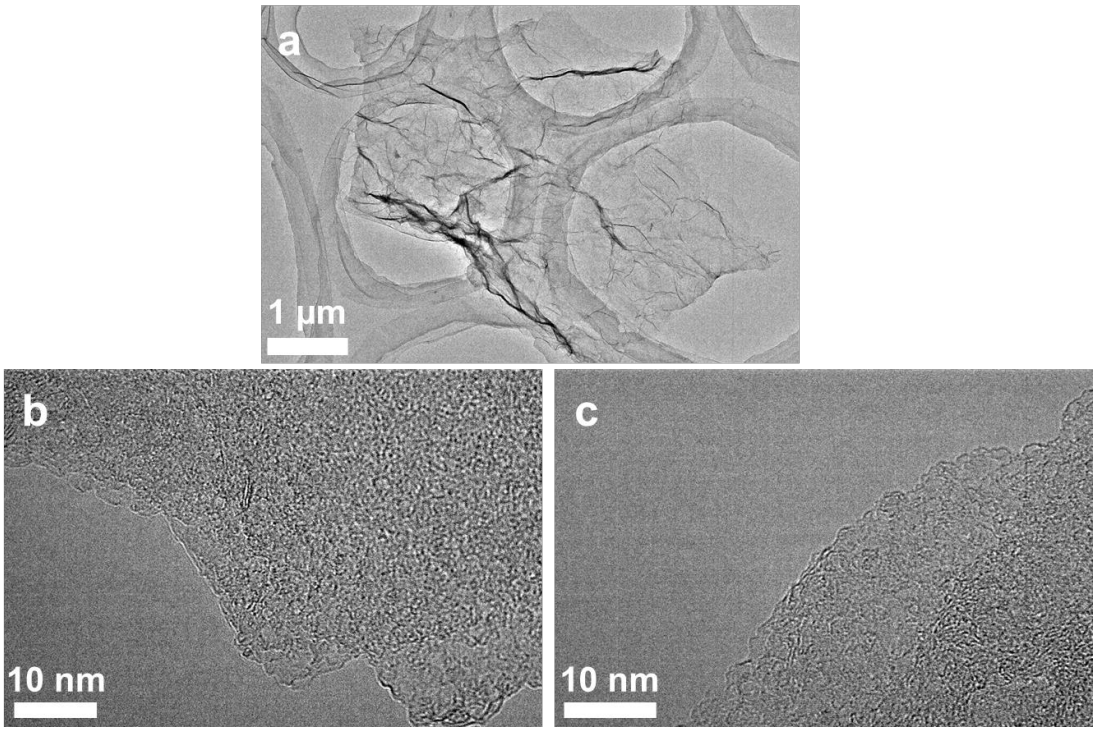

Figure S9

The TEM image **(a)** indicates that the size of graphene sheet was larger than several μm^2 and high-magnification TEM images **(b)** and **(c)** show that most regions of the graphene sheets were monolayer[23].

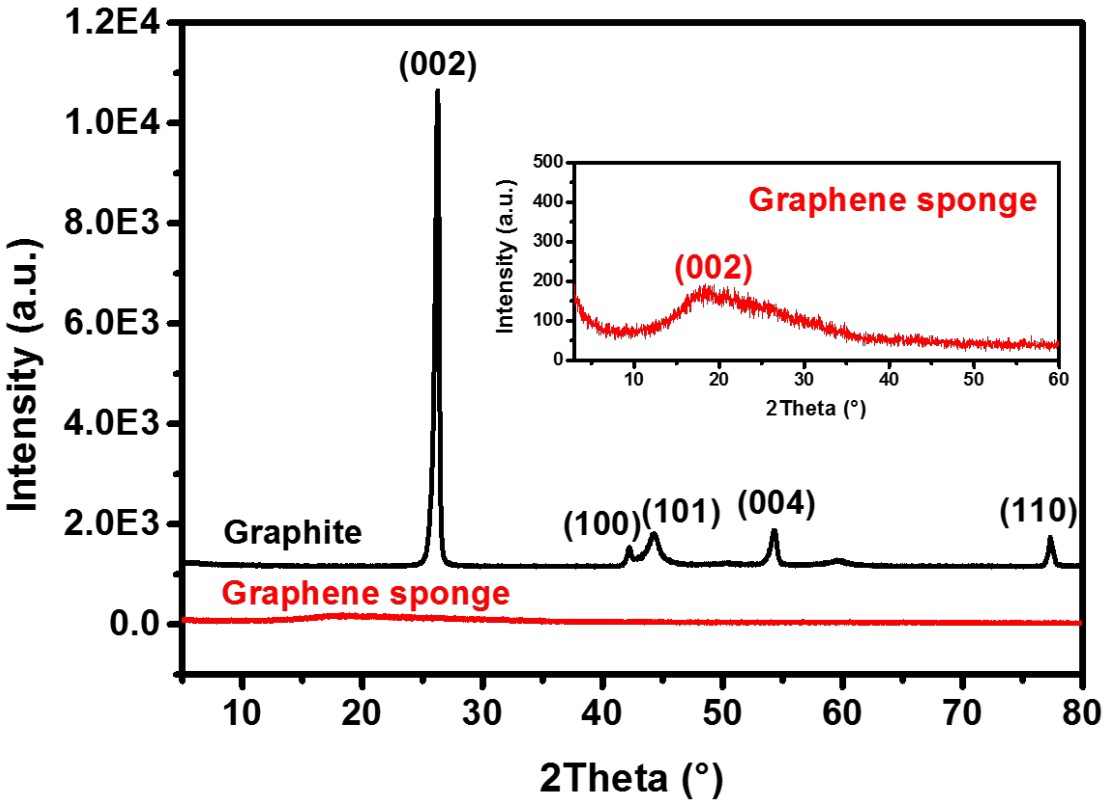

Figure S10

The XRD results of graphene sponge (red line) and graphite (black line) as the comparison. Compared with graphite, graphene sponge exhibits a very weak and extremely broad (002) peak, indicating almost no or very weak long-range graphene sheet re-stacking.

DOI: 10.1038/NPHOTON.2015.105

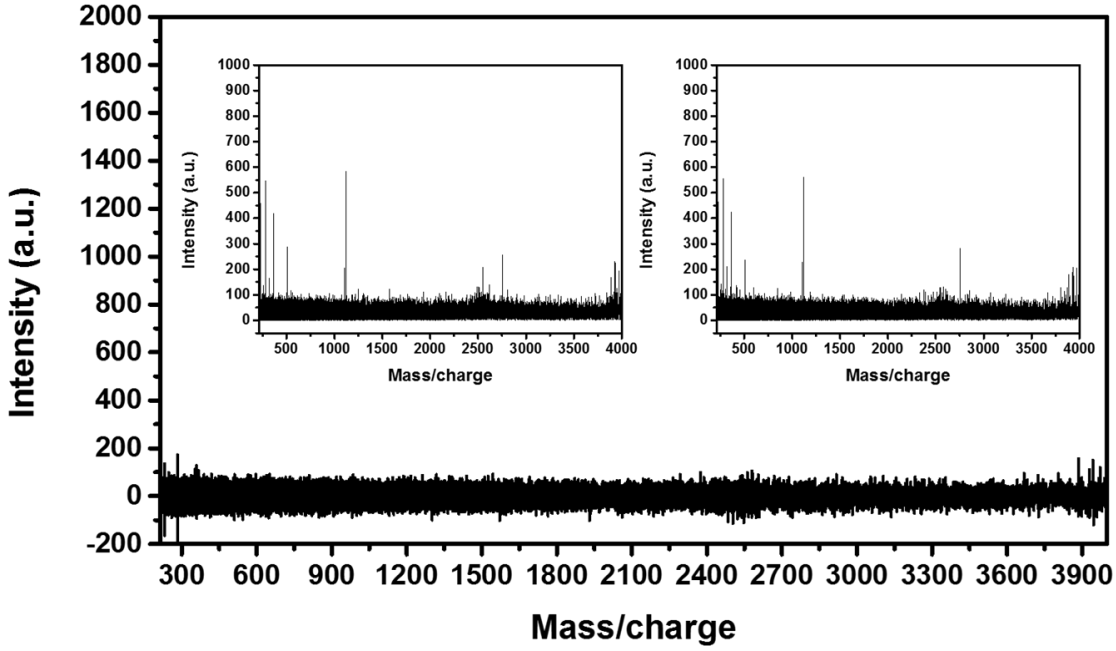

Figure S11

Modified mass spectrum obtained by a MALDI-FTICR mass spectrometer. Top right inset was the mass spectrum obtained from the graphene sponge illuminated only by our Watt level continuous wave laser (the pulse laser of MALDI source was turned off), and top left inset was the recorded blank noise (without laser illumination and other experiment conditions were all the same). The subtractive spectrum showed in the main panel indicates that no carbon clusters or other small molecular pieces/particles were detected under the instrument detection limit (several ppm). The test mode was positive and the mass/charge range was from 216 to 4000.

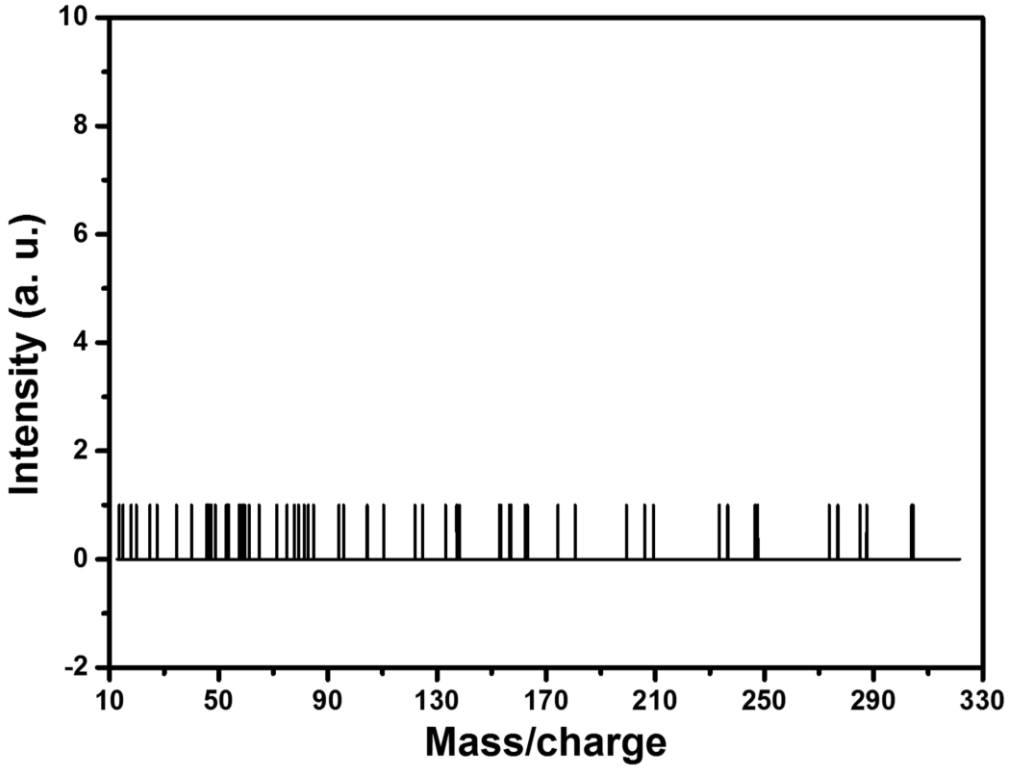

Figure S12

The mass spectrum obtained by a non-commercial OA-TOF mass spectrometer. The mass spectrum obtained from the graphene sponge indicates that no molecule or particle was detected in the mass range of 12-321 amu under the same laser illumination condition under the instrument detection limit (ppm level).

DOI: 10.1038/NPHOTON.2015.105

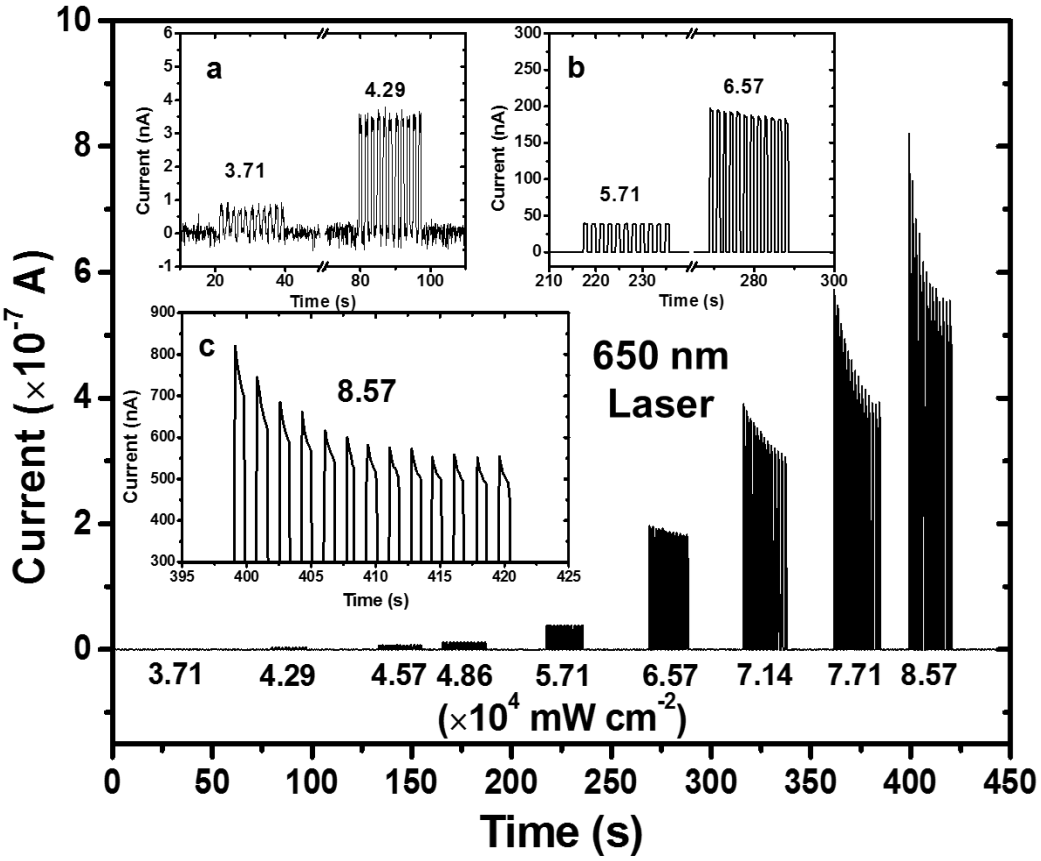

Figure S13

A whole current curve graph recorded for the graphene sponge under the illumination of a 650 nm laser. The intensity of each group signals increased distinctly with the increasing laser power density. Three insets **(a, b, c)** were the enlarged images of corresponding regions for better reading of the main graph. When the laser power density was relatively small, the Signal/Noise Ratio was poor **(a)**. When the laser power density was moderate, the current signal was smooth and stable with different pulses **(b)**. When the laser power density was large enough, the intensity of each current signal under the same laser power density became slightly weaker with different pulses **(c)**, possibly due to the increased positive charge on the sample. The laser spot area was ~3.5 mm^2.

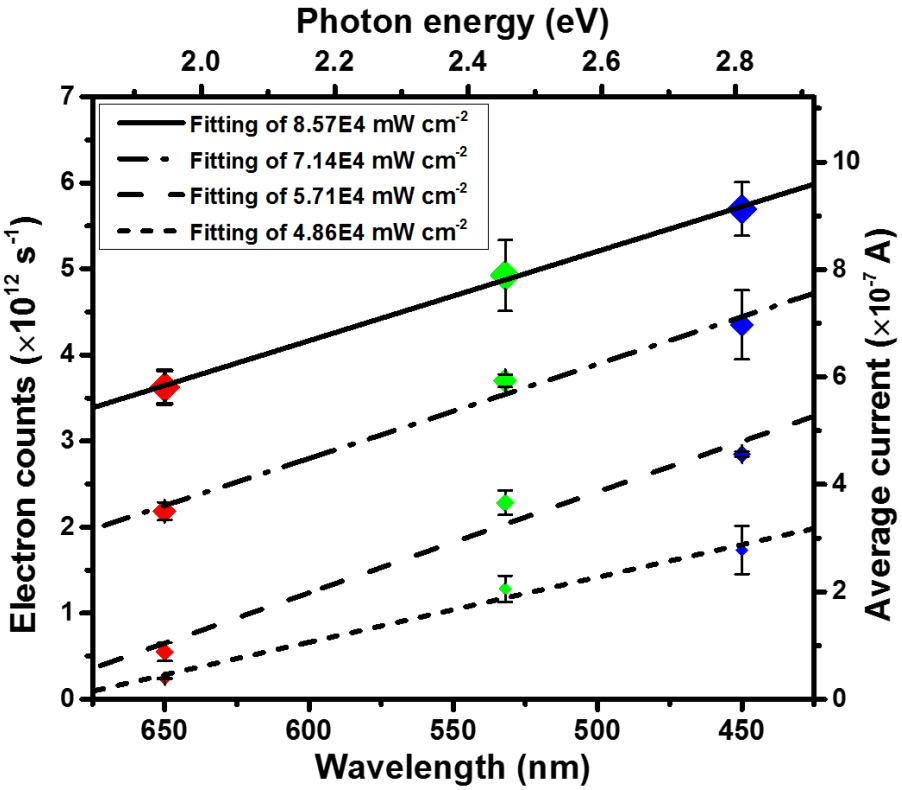

Figure S14

The linear relationship of the ejected electron counts per unit time (and average current) with the laser wavelength (and the photon energy) under the same laser power density. (450 nm: blue diamonds; 532nm: green diamonds; 650nm: red diamonds; bigger size of the diamond means higher laser power density.) The error bars represented the Standard Deviation (SD) from all the repeated tests under a given condition. The laser spot areas were all about 3.5 mm^2.

DOI: 10.1038/NPHOTON.2015.105

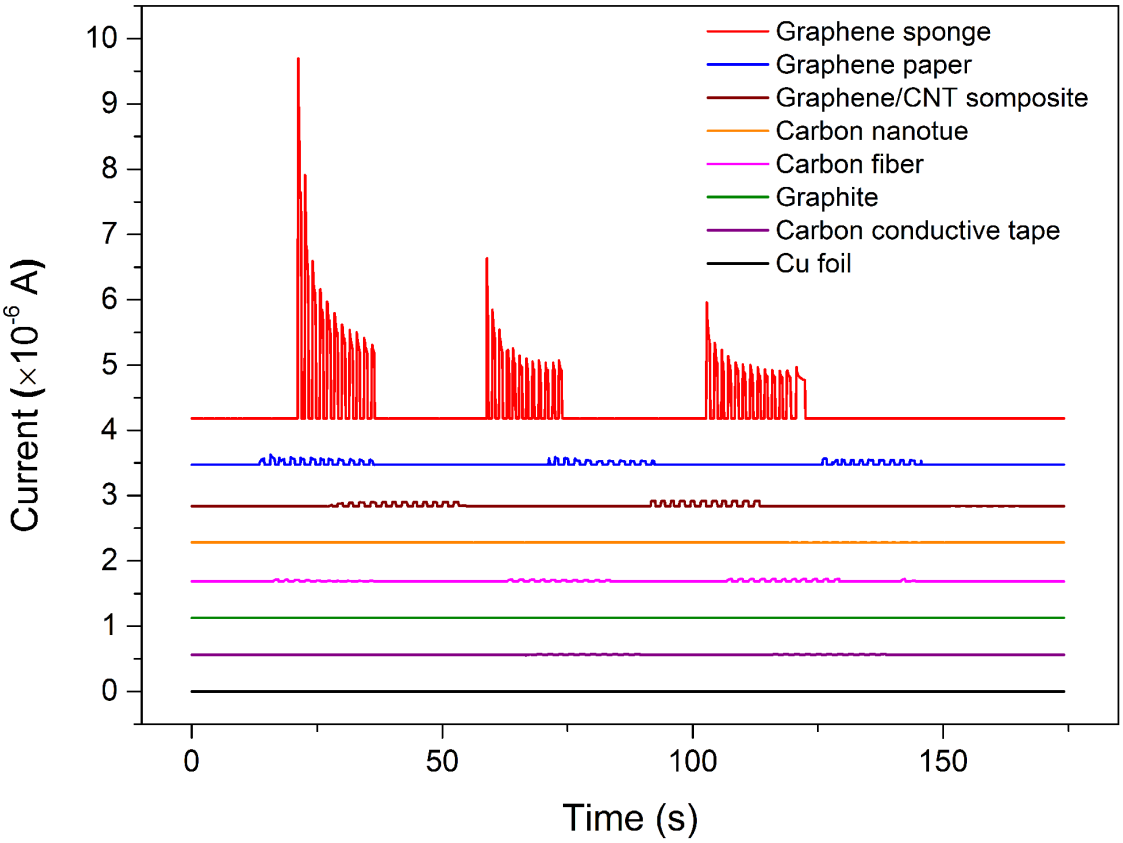

Figure S15

Emitted electrons measurement of different materials compared with graphene sponge. Under the same experimental conditions, all these control materials have neglectable current signals. The laser wavelength was 450 nm and the power was 3 W (~8.57 × 10^4 mW cm^{-2}).

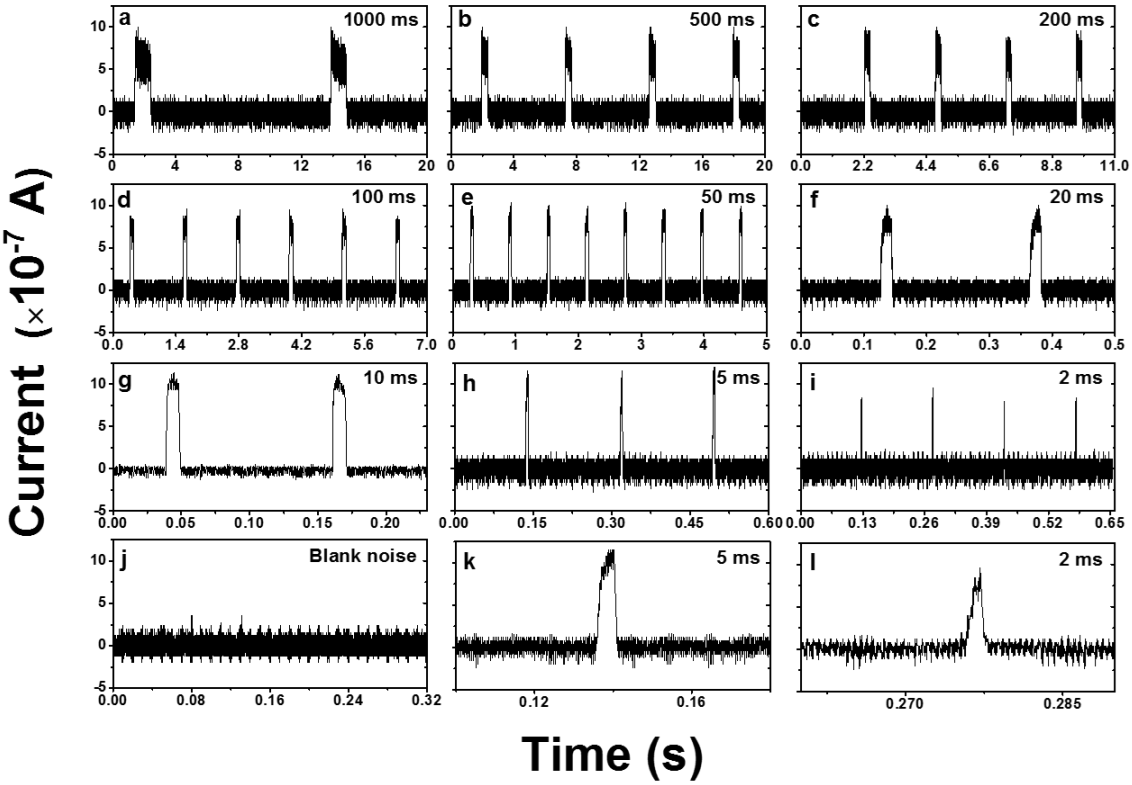

Figure S16

The current signals recorded under the illumination of laser pulse with different pulse widths ranged from 1000 to 2 ms. The laser wavelength was 450 nm and the power density was 3 W (~8.57 × 10^4 mW cm^{-2}). A digital oscilloscope with high enough sampling frequency was used to record the current in real time. No time-related delay impact was observed in the cycling test with different laser pulse widths from 1000–2ms, and no meaningful current intensity change was observed either with different laser pulse widths (a–i). The slight difference between different signals should be caused by measurement error. The panels in the bottom row were the recorded blank noise without laser illumination (j), enlarged views of signals of 5 (k) and 2 (l) ms laser pulses respectively. These results exclude a dominant role for the conventional thermionic mechanism.

DOI: 10.1038/NPHOTON.2015.105

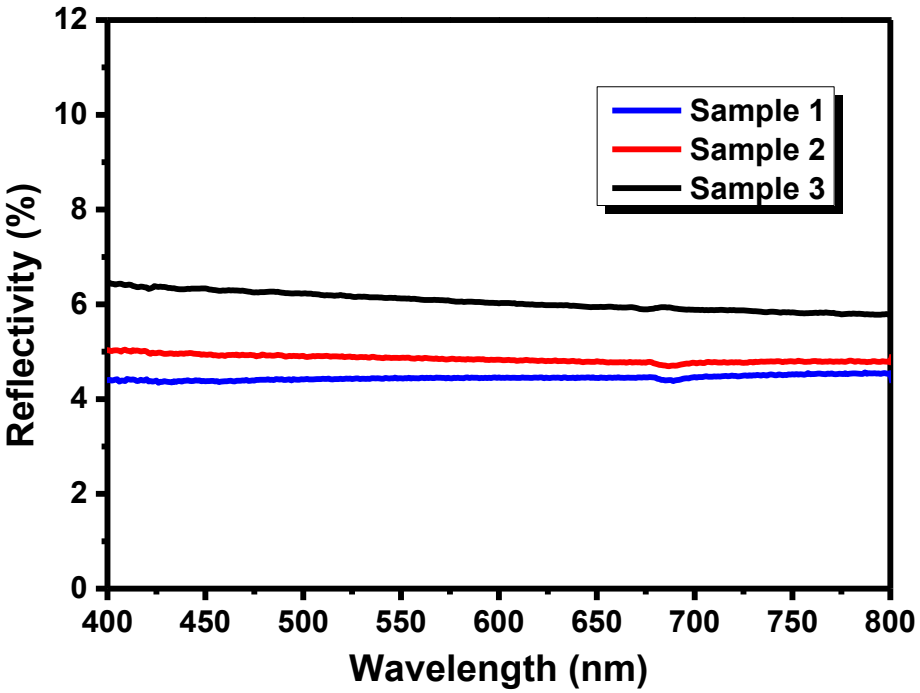

Figure S17

Vis-DRS results of three different graphene sponge samples. The graphene sponge had a quite low reflectivity in the measured range from 400 to 800 nm, and three samples gave almost the same results. The average reflectivity was ~ 0.05.

Table S1

The mass content, mass ratio and atomic ratio of C and O elements obtained by EA, EDS, XPS and AES. The carbon content of graphene sponge is > 93 wt. %.

	wt.% C	wt.% O	wt.% H	C/O mass ratio	C/O atomic ratio
EA	**93.54**	**5.14**	**1.32**	**18.10**	**24.26**
EDS	**93.58**	**6.42**	**—**	**14.60**	**19.44**
XPS	**93.38**	**6.82**	**—**	**13.69**	**18.26**
AES	**93.55**	**6.45**	**—**	**14.50**	**19.34**

DOI: 10.1038/NPHOTON.2015.105

Supplementary Video (S1-S5) Captions

Video S1

Horizontal propulsion of graphene sponge by laser. The graphene sponge sample was placed in a horizontal quartz tube (internal diameter d = 15 mm) which connected with a molecular pump. The vacuum was better than 5.3×10^{-6} Torr. The cylinder shape sample mass was 0.25 mg, the diameter and thickness were 12 and 2 mm respectively. The lasers wavelengths used were 450, 532 and 650 nm respectively. The laser powers were all 3 W and the laser spot areas were ~4 mm^2. The video shows the graphene sponge sample could be propelled immediately when laser beam was illuminated on it. Lasers with different wavelengths gave the similar result.

Video S2

Vertical upwardly propulsion of graphene sponge by laser. The sample was placed in a glass tubule (internal diameter d = 5 mm), and the glass tubule was put in the quartz tube (internal diameter d = 15 mm) which acted as a vacuum container. The tubule was used to prevent the sample from running randomly. The vacuum was better than 5.3×10^{-6} Torr. The lasers wavelengths used were 450, 532 and 650 nm respectively. The laser powers were all 3 W and the laser spot areas were ~4 mm^2. The sample mass was 0.08 mg, the diameter and height were 4 and 6 mm respectively. The video shows that the graphene sponge could be vertical upwardly propelled by lasers with different wavelength. A shorter wavelength laser could propel the graphene sponge higher and more effectively.

Video S3

Vertical and horizontal propulsion of graphene sponge by a short-arc xenon lamp. The sample was placed in a quartz tube (internal diameter d = 15 mm) which connected with a molecular pump. The vacuum was better than 5.3×10^{-6} Torr. The cylinder shape sample mass was 0.25 mg, and the diameter and thickness were 12 and 2 mm respectively.

Video S4

Horizontal propulsion of graphene sponge by focused real sunlight. The video was taken on the building roof on a sunny day. By using a Fresnel lens to focus the real sunlight, the graphene sponge sample could be propelled directly by sunlight. The vacuum of the tube was 6.8×10^{-4} Torr. The intensity of the focused sunlight was in the range from a few to tens of AM. The diameter and height of the sample was 10 and 11 mm respectively, and the sample mass was 0.88 mg.

Video S5

Rotation of the graphene sponge by laser. The experiment setup was shown in Fig. 2a. The graphene sponge was cut into a cuboid ($12 \times 7 \times 5$ mm^3) and the mass was 0.44 mg. A glass capillary was used to act as an axis to penetrate through the center of the sample. The whole device was put on a polytetrafluoroethylene (PTFE) plate which was placed in a quartz container to obtain the required vacuum environment. The vacuum was 6.8×10^{-4} Torr. The laser wavelengths were 450, 532 and 650 nm respectively, and the laser powers were all 1 W with spot areas at ~ 4 mm^2. We used a non-contact tachometer to measure the rotation speed.

DOI: 10.1038/NPHOTON.2015.105

References

S1. Becerril, H. A. *et al.* Evaluation of solution-processed reduced graphene oxide films as transparent conductors. *ACS Nano* **2**, 463-470 (2008).

S2. Ashkin, A. History of optical trapping and manipulation of small-neutral particle, atoms, and molecules. *IEEE J. Sel. Top. Quantum Electron.* **6**, 841-856 (2000).

S3. Han, L.-H. *et al.* Light-powered micromotor driven by geometry-assisted, asymmetric photon-heating and subsequent gas convection. *Appl. Phys. Lett.* **96**, 213509 (2010).

S4. Kopp, G. & Lean, J. L. A new, lower value of total solar irradiance: evidence and climate significance. *Geophys. Res. Lett.* **38**, L01706 (2011).

S5. Leipold, M. *et al.* Solar sail technology development and demonstration. *Acta Astronaut.* **52**, 317-326 (2003).

S6. Nair, R. R. *et al.* Fine structure constant defines visual transparency of graphene. *Science* **320**, 1308 (2008).

S7. Fang, T., Konar, A., Xing, H. & Jena, D. Mobility in semiconducting graphene nanoribbons: phonon, impurity, and edge roughness scattering. *Phys. Rev. B* **78**, 205403 (2008).

S8. Fang, T., Konar, A., Xing, H. & Jena, D. High-field transport in two-dimensional graphene. *Phys. Rev. B* **84**, 125450 (2011).

S9. Jauregui, L. A. *et al.* Thermal transport in graphene nanostructures: experiments and simulations. *ECS Trans.* **28**, 73-83 (2010).

S10. McAllister, M. J. *et al.* Single sheet functionalized graphene by oxidation and thermal expansion of graphite. *Chem. Mater.* **19**, 4396-4404 (2007).

S11. Zakharchenko, K., Katsnelson, M. & Fasolino, A. Finite temperature lattice properties of graphene beyond the quasiharmonic approximation. *Phys. Rev. Lett.* **102**, 046808 (2009).

S12. Eda, G. & Chhowalla, M. Chemically derived graphene oxide: towards large-area thin-film electronics and optoelectronics. *Adv. Mater.* **22**, 2392-2415 (2010).

S13. Kudin, K. N. *et al.* Raman spectra of graphite oxide and functionalized graphene sheets. *Nano Lett.* **8**, 36-41 (2008).

S14. Paredes, J. I., Villar-Rodil, S., Solis-Fernandez, P., Martinez-Alonso, A. & Tascon, J. M. Atomic force and scanning tunneling microscopy imaging of graphene nanosheets derived from graphite oxide. *Langmuir* **25**, 5957-5968 (2009).

S15. Su, C.-Y. *et al.* Electrical and spectroscopic characterizations of ultra-large reduced graphene oxide monolayers. *Chem. Mater.* **21**, 5674-5680 (2009).

S16. Yung, K. C. *et al.* Laser direct patterning of a reduced-graphene oxide transparent circuit on a graphene oxide thin film. *J. Appl. Phys.* **113**, 244903 (2013).

S17. Zhan, D. *et al.* Electronic structure of graphite oxide and thermally reduced graphite oxide. *Carbon* **49**, 1362-1366 (2011).

S18. Haerle, R., Riedo, E., Pasquarello, A. & Baldereschi, A. sp^2/sp^3 hybridization ratio in amorphous carbon from C 1*s* core-level shifts: X-ray photoelectron spectroscopy and first-principles calculation. *Phys. Rev. B* **65**, 045101 (2001).

S19. Okpalugo, T., Papakonstantinou, P., Murphy, H., McLaughlin, J. & Brown, N. High resolution XPS characterization of chemical functionalised MWCNTs and SWCNTs. *Carbon* **43**, 153-161 (2005).

S20. Gardner, S. D., Singamsetty, C. S., Booth, G. L., He, G.-R. & Pittman Jr, C. U. Surface characterization of carbon fibers using angle-resolved XPS and ISS. *Carbon* **33**, 587-595 (1995).

S21. López, G. P., Castner, D. G. & Ratner, B. D. XPS O 1s binding energies for polymers containing hydroxyl, ether, ketone and ester groups. *Surf. Interface Anal.* **17**, 267-272 (1991).

S22. Wu, Y. *et al.* An isotropic spongy graphene bulk material with both super compressive elasticity and near-zero Poisson's ratio. *Nature Commun.* **6**, 6141 (2015).

S23. Meyer, J. C. *et al.* The structure of suspended graphene sheets. *Nature* **446**, 60-63 (2007).